Astronomy
&
Astrophysics

Very compact radio emission from high-mass protostars

I. CRL 2136: Continuum and water maser observations

K. M. Menten and F. F. S. van der Tak

Max-Planck-Institut für Radioastronomie, Auf dem Hügel 69, 53121 Bonn, Germany

Abstract. We report 5–43 GHz radio observations of the CRL 2136 region at $0\rlap{.}''6$–$6''$ resolution. We detect weak (mJy intensity) radio emission from the deeply embedded high-mass protostar IRS 1, which has an optically thick spectrum up to frequencies of 22 GHz, flattening at higher frequencies, which might be explained by emission from a jet. Water maser mapping shows that the strong emission observed redshifted relative to the systemic velocity is spatially coincident with the optically thick continuum emission. The H_2O maser emission from this object (and others we know of) seems to have a different origin than most of these masers, which are frequently tracing bipolar high-velocity outflows. Instead, the CRL 2136 H_2O emission arises in the close circumstellar environment of the protostar (within 1000 AU). We speculate that most of it is excited in the hot, dense infalling gas after the accretion shock, although this cannot explain *all* the H_2O emission. An accretion shock nature for the continuum emission seems unlikely.

Key words. ISM: molecules – stars: circumstellar matter – stars: formation

1. Introduction

For the earliest, deeply embedded phases of high-mass star formation, the distribution and kinematics of material on $\lesssim$1000 AU scales is poorly known, due to the large ($\gtrsim$1 kpc) distances involved, and the lack of tracers at optical and near-infrared wavelengths. The first systematic description of this phase was presented in a classic paper by Willner et al. (1982), which discussed 2–13 μm spectra of a sample of 19 compact infrared sources associated with molecular clouds already coined as "protostars". Observations of these sources by Mitchell et al. (1990) indicated large column densities of CO, spread over multiple temperature and velocity components. In addition, Mitchell et al. (1991) and others discovered strong outflows with velocities up to 70 km s^{-1} in CO and/or H_2O maser emission and up to 200 km s^{-1} in infrared CO absorption.

Observations with the Infrared Space Observatory (ISO) Short-Wavelength Spectrometer (SWS, see, e.g., van Dishoeck et al. 1998) have refined our view on the structure and composition of the Willner et al. sources. The ISO data suggest an evolutionary sequence starting with cold, ice-rich objects such as W33A and NGC 7538 IRS9, and going toward warm sources like GL 2591 where gas/solid molecular abundance ratios are $\gg$1. Submillimeter maps (van der Tak et al. 2000b) indicate large masses of these envelopes, and a relation between temperature and the ratio of envelope mass to stellar mass. Additional data on this evolutionary sequence comes from submillimeter spectroscopy (van der Tak et al. 2000a, 2003), although the lines are more than an order of magnitude weaker than in the Orion "Hot Core", the prime example of its class, which is more evolved and less distant.

Despite this progress, not much is known yet about the small-scale structure and kinematics of embedded high-mass protostars. How do the observed outflows start? How do they interact with their environment on <1000 AU scales? Subarcsecond resolution observations are necessary to shed light on these and other questions, which, at (sub)mm wavelengths, will begin to be addressable with the Submillimeter Array (Moran 1998), but for the high brightness sensitivities needed will have to await the Atacama Large Millimeter Array (ALMA[1]).

Centimeter-wavelength radio emission penetrates dust and can *now* be studied at these interesting resolutions with instruments such as the Very Large Array (VLA). Medium-sensitivity (few mJy level) VLA surveys of many high-mass star-forming regions were made in the last 15 years at high (sub-arcsecond) resolution (e.g., Wood & Churchwell 1989). Subsequent (sub)millimeter-wavelength molecular line observations have established that in the ultracompact HII region (UCHII) region phase young high-mass stars are still

---

[1] `http://www.eso.org/projects/alma/` or
`http://www.alma.nrao.edu/`

surrounded by massive, dense, and hot molecular cores (Garay & Lizano 1999).

However, also found were a number of submillimeter sources undetected at cm-wavelengths at the sensitivity levels of the mentioned surveys, which, however from their IRAS colours, derived temperatures, densities, and dimensions were virtually indistinguishable from those associated with UCHII regions (e.g., Molinari et al. 1996, 1998, 2000; Sridharan et al. 2002; Beuther et al. 2002a) . Sensitive VLA observations led to the detection of weak radio emission in some of these sources, which, in the case of the Turner-Welch object near the UCHII region W3(OH), surprisingly, turned out to be of non-thermal nature and exhibits a jet-like shape (Reid et al. 1995; Wilner et al. 1999). In other cases, weak, up to (at least) 7 mm wavelength optically thick, "hypercompact" HII regions were found (e.g., Tieftrunk et al. 1997; Churchwell 2002). In the Orion-KL region, one such source ("I") was found to be jet-like and have a thermal spectrum (see Menten & Reid 1995 and below).

A basic motivation for searching compact radio continuum emission within high-mass protostellar cores is to precisely locate the position of the exciting sources, a critical requirement nowadays, as adaptive optics techniques deliver infrared observations with resolutions similar to the those of the interferometric radio data. Of equal or even more importance is the fact that the sheer existence of the radio continuum emission and its observed spectrum constrains theoretical models.

A forthcoming paper (van der Tak & Menten, in prep.) summarizes existing radio data of high-mass protostars and presents new observations of such and similar sources.

In this paper we consider the case of CRL 2136[2], evolution-wise an intermediate case between W33A and GL 2591. Multi-wavelength near-infrared (NIR) imaging by Kastner et al. (1992) revealed a triple source structure, surrounded by nebulosity, which they whimsically named the "Juggler Nebula". Their IR-polarimetry led Kastner et al. to suggest that a deeply embedded source in the westernmost part of the triple structure, IRS 1, was the dominating energy source, providing $5 \times 10^4 \, L_\odot$ to the region, for which they derive a kinematic distance of 2 kpc.

This paper reports successful multi-radio wavelength searches for weak continuum emission from CRL 2136. At our highest observing frequency (43.3 GHz) we resolve the emission. We also present maps of the unusually compact water maser emission distribution associated with the source.

In Sect. 2 we describe the reduction of archival VLA continuum and 22.2 GHz H$_2$O maser line data of CRL 2136 and present the results. In Sect. 3 we discuss these results in the context of other phenomena found in the region in question. We also claim that the H$_2$O masers in this source belong to a class up to now not recognized, that is excited in the innermost circumstellar regions rather, as most water masers, in outflows further out.

2. VLA observations, data reduction and results

2.1. Archival continuum and water data

The archival CRL 2136 data discussed here were retrieved from the NRAO[3] Very Large Array (VLA) archival database (project name: AK 297, observing date: 1992 May 19, when the VLA was in its C-configuration). Three continuum uv-databases were obtained. Each had data taken with 2 intermediate frequency (IF) bands of width 2 × 50 MHz each centered ±25 MHz of 4.8601, 8.4399, and 14.9399 GHz. (These band are termed C-, X-, and U-band in radio astronomy lingo.) In addition, a 127 channel spectral line database was used, containing a 15 min duration snapshot of the H$_2$O maser line at 22.23508 GHz toward CRL 2136 (which is in "K"-band). Each of the channels was of 12.2 kHz width, corresponding to 0.165 km s^{-1} and the total velocity coverage was 20.8 km s^{-1}, centered at an LSR velocity of 26.3 km s^{-1} and, thus, covered −6.9 to +13.9 km s^{-1} around the systemic velocity, which is 22.8 km s^{-1} (van der Tak et al. 2000b).

The data were edited, calibrated, and imaged in the "usual" way with NRAO's Astronomical Image Processing System (AIPS). In the case of the spectral-line data, the "channel 0" database, comprising the inner 75% of the passband, was used for this. Absolute calibration was obtained from observations of 3C286 using the fluxes interpolated from the values given by Baars et al. (1977). NRAO 530 was the phase calibrator. Unfortunately, no 22.2 GHz data exist for 3C286. To achieve absolute calibration for the K-band data we determined NRAO 530's flux density at that 22.2 GHz by extrapolation using the spectral index, α_{XU}, determined from its X- and U-band flux densities. The error in the absolute calibration should be within 10%.

Restoring beam major and minor axes and position angles (PAs, east of north) were (7.″7, 4.″5, 18°), (4.″3, 2.″5), (2.″4, 1.″5, 6°) for the C-, X-, and U-band maps, respectively.

2.2. Effelsberg water observations

A spectrum of the H$_2$O maser line was taken in position-switching mode with the MPIfR 100 m telescope near Effelsberg, Germany. A K-band HFET receiver was used and the spectrometer was an autocorrelator.

2.3. New VLA continuum data

New VLA data were taken on two dates: On 2001 September 09 in C-configuration and on 2002 March 23 in A-configuration. This time observations were made in the highest ("Q") VLA frequency band. On both dates, data were taken with 2 intermediate frequency (IF) bands of width 2 × 50 MHz each centered ±25 MHz of 43.3399 GHz. Absolute and phase calibration and data processing was performed as described above, with the difference that short (duration ~70 s) scans of CRL2136 were alternated with 10 s duration scans of the

---

[2] Also known as AFGL 2136 or GL 2136; l, b = 17.°639, +0.°16.

nearby calibrator 18 296−10 374, with a 20 s "dead time" in between (needed for slewing). As proven a posteriori by the quality of the resulting images, this fast "switching" provided for near-perfect calibration. For absolute calibration 3C286 was observed. Q-band observations are more affected by variations in the weather conditions and gain variations with telescope elevation than lower frequency observations. Therefore, we estimate a 30% uncertainty for our Q-band flux densities.

Restoring beams were (0.''61, 0.''43, −2°) and (0.''057, 0.''041, 7°) for the Q-band C- and A-array maps, respectively.

2.4. Continuum results

At 4.9, 8.4, and 14.9 GHz we produced large maps of size 2048''×2048'' around the phase center position of $(\alpha, \delta)_{J2000} =$ 18^{h}22^{m}26.^{s}482, −13°30'13.''1. At 43.3 GHz only a small map of extent (6.''4, 6.''4) was made. Table 1 lists the sources detected (using the multiple-peak-finding AIPS task SAD) with more than 5 times the 1σ rms noise levels of 0.16, 0.046, and 0.14 mJy beam^{-1} in the C-, X-, and U-band maps. The flux densities are corrected for primary beam response. The errors in Table 1 are statistical errors delivered by SAD added quadratically to the absolute errors of 0.''1 determined as follows. To obtain a "realistic" estimate of the absolute position errors remaining after phase calibration, we "calibrated" the NRAO 530 data "with" the 3C286 data. The resulting position differed from 3C286's nominal position by $(\theta_x, \theta_y) = $ (+0.''08, −0.''66), (+2.''0, +0.''62), and (0.''54, −0.''24) at C-, X-, and U-band, respectively. Since the arc between NRAO 530 and CRL 2136 is more than 50 times greater than that between NRAO 530 and CRL 2136, we feel safe to assume that the errors in the positions in Table 1 are smaller that 0.1 arcsec. Rather than indicating that radio sources 1, 2, 3, and 5 in Table 1 are marginally resolved, the slightly higher numerical values of the integrated flux densities than the peak values are most likely caused by residual phase errors; self calibration was not possible due to the weakness of the emissions. Three radio sources (RS 1, 2, and 5) are detected at 4.9 GHz only and one (RS 3) at 8.4 GHz only. As shown in Fig. 1, only RS 3 and 4 are in the immediate vicinity of IRS 1.

2.4.1. Radio source 4

Using JMFIT, we determine Q-band peak (S_p) and integrated (S_i) intensities of 4.49 (0.22) mJy beam^{-1} and 4.20 (0.36) mJy, respectively, for the C-array data and 1.43(0.10) mJy beam^{-1} and 1.78(0.21) mJy for the A-array data. The discrepancy between the A- and C-array fluxes is larger than our assumed error margin and is possibly due to source variability. We produced a source model, derived from a Gaussian fit to our (lower resolution) C-band data and introduced it in the A-array u, v-database, imaged it and made a Gaussian fit to the model source flux distribution in the A-array map. We retrieved *all* the input flux. We therefore are certain that we are not "resolving out" any extended structure and have great confidence about the quality of our phase calibration.
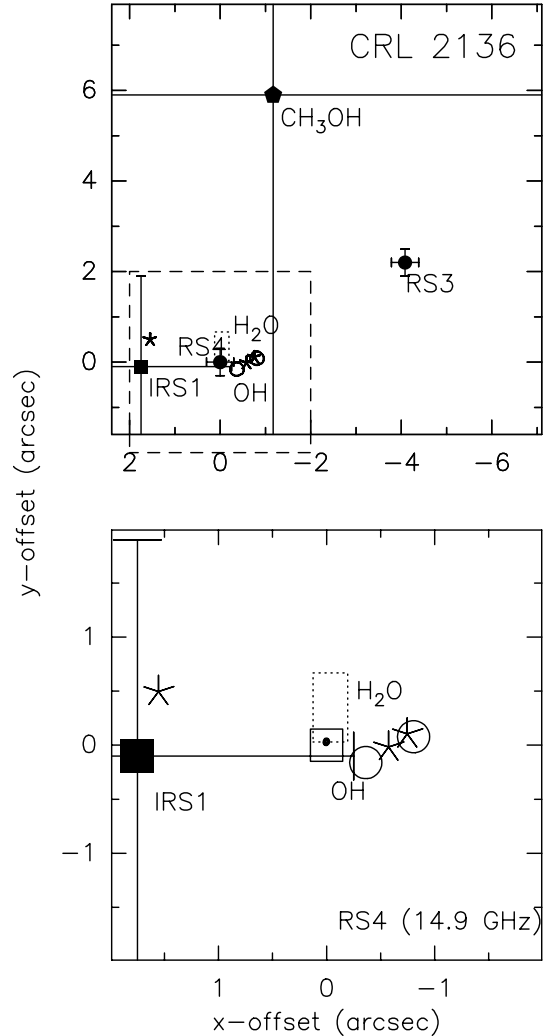

Fig. 1. Objects in the CRL 2136 region: the *upper panel* shows the positions of radio sources 3 and 4 *(filled circles)*, infrared source 1 *(filled square)*, and the class II CH$_3$OH maser *(filled pentagon)*. The three little stars mark the positions from which of 1665 MHz RCP maser emission arises and the circles mark LCP emission. For the OH emission, the symbol sizes reflect the 0.''3 position uncertainties. The (at this scale) unresolved dot at the (0, 0) position represents the Q-band map of RS 4, an enlarged image of which is shown in Fig. 2. The square around it indicates its 0.''3 position uncertainty. The *dotted rectangle* outlines the region containing H$_2$O maser emission shown in detail in Fig. 4 and the *dashed rectangle* outlines an enlarged region shown in the *lower panel*.

JMFIT statistics yields the source properties listed in Table 2 with formal errors. The dimensions in the table should probably taken as an upper limit on the actual source size. Figure 2 illustrates these results. The shape (elongation) and size as well as its radio luminosity and spectral index make RS 4, which is of central interest to this paper, strikingly similar to source I in the Orion-KL region (see Table 2 and discussion below).

Table 1. Radio and infrared emission from CRL 2136.

Source	α_{2000} 18^h22^m	δ_{2000} $-13°$	$\sigma(\alpha,\delta)$ (arcsec)	$S_{p,4.9}$ (mJy b^{-1})	$S_{i,4.9}$ (mJy)	$S_{p,8.4}$ (mJy b^{-1})	$S_{i,8.4}$ (mJy)	$S_{p,14.9}$ (mJy b^{-1})	$S_{i,14.9}$ (mJy)
RS 1	$17\overset{s}{.}22$	$27'41\overset{''}{.}4$	0.3	3.1(0.2)	4.5(0.5)	<0.14	–	<0.42	–
RS 2	22.11	33 18.5	0.4	1.9(0.2)	2.9(0.5)	<0.14	–	<0.42	–
RS 3	26.10	30 09.7	0.3	<0.48	–	0.63(0.08)	0.69(0.16)	<0.5	–
CH_3OH	26.3	30 06	10						
RS 4	26.37	30 11.9	0.3	<0.48	–	0.56 (0.08)	0.56 (0.08)	0.99(0.13)	1.30(0.27)
H_2O	26.38	30 11.8	0.1						
IRS 1	26.5	30 12	2						
RS5	39.209	29 56.36	0.2	9.0(0.2)	9.1(0.3)	<0.4	–	<0.5	–

[a] $S_{p,\nu}$ and $S_{i,\nu}$ are the peak and integrated flux densities, respectively, and their *formal* errors determined with the AIPS task JMFIT. The *absolute* flux density calibration should have uncertainties of less than 10% at *C*, *X*, and *U*-band and ≲20% at *K*- and ≲30% at *Q*-band. Upper limits are 3 times the 1σ rms noise. Radio position errors are formal errors from JMFIT with the estimated absolute position error of 0.1 arcsec quadratically added. The error in the average H_2O maser position is completely dominated by the latter. This "average" H_2O position is the variance-weighted mean position of the Gaussian fit results to the velocity channels with strong (>10 Jy) emission, i.e., from 26.5 to 27.9 km s^{-1}. RS 4 is also detected at 43 and 86 GHz at a position consistent with that given above (see Table 2). See reference in text for the CH_3OH maser position.
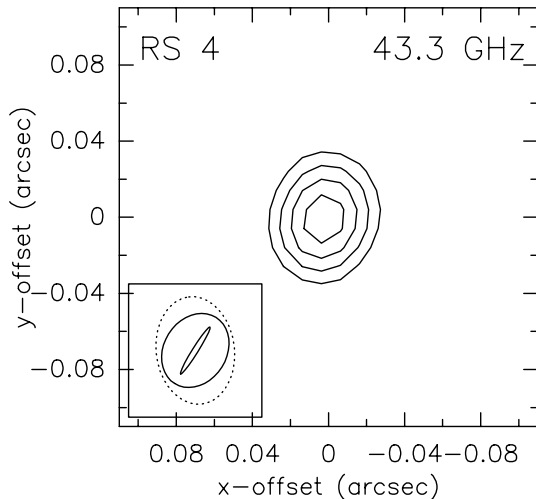

Fig. 2. Radio source 4 at 43.3 GHz: the contours represent 5, 7, 9, and 11 times the 2.7 mJy beam^{-1} rms noise in our 43.3 GHz map. The *dotted ellipse* in the *lower left* corner represents the FWHM size of the Gaussian restoring beam, while the *full line* ellipses represent the maximum and nominal FWHM source size from JMFIT (see discussion in text). Angular offsets are relative to the position given in Table 1.

2.5. Water results

In the water line, a $25\overset{''}{.}6 \times 25\overset{''}{.}6$-sized map was made of the channel with the strongest emission (at 27.1 km s^{-1}). After several iterations of self calibration a 390 Jy strong feature was obtained. The phase and amplitude corrections were copied to the other velocity channels.

A spectrum at the pixel with maximum emission was made and is shown in Fig. 3. The peak emission is comparable in strength to the 330 Jy Valdettaro et al. (2001) report between 23 and 31 km s^{-1}; the weak emission we observe outside that range is below their sensitivity limit. Their velocity of peak emission, $v_{\mathrm{peak}} = 27.1$ km s^{-1}, coincides exactly with ours, which is remarkable, since their observation was made

on 2000 January 18, almost 8 years after the VLA data discussed here were taken. On 1991 January 31, Kastner et al. (1992) also detect a single feature (of 46 Jy flux density), however at $v_{\mathrm{LSR}} = 26.3 \pm 0.1$ km s^{-1}. The Effelsberg spectrum has its peak emission at 27.0 km s^{-1}. In some sources H_2O maser spectra vary significantly on timescales as short as days and it is worth noting that the "stability" of a H_2O maser spectrum observed toward CRL 2136 appears unique and has to be considered when modeling the emission.

While in the VLA spectrum, all of the strong emission is redshifted relative to the systemic velocity, the Effelsberg spectrum shows redshifted (between 24.6 and 28.8 km s^{-1}) as well as moderately strong blueshifted emission (between 16.7 and 21.7 km s^{-1}) at our 5σ noise level of 0.8 Jy and nothing between nor outside of these velocity intervals.

In Fig. 4 we present the results of Gaussian position fitting (using the AIPS task JMFIT). Since the total spatial spread of the emission is all within a synthesized beamwidth, only a single Gaussian was fitted to each channel. Each cross presents the position and 1σ error bars of the emission in one channel. The arrows underneath the spectrum (Fig. 3) mark parts which were averaged before mapping. The emission from these velocities falls in the same general region as the stronger emission mapped individually, i.e., the $0\overset{''}{.}3 \times 0\overset{''}{.}5$ (600×1000 AU) region around the variance-weighted mean position which is given in Table 1. Based on our experience with the lower-frequency data described below, we estimate that the "real" *absolute* position uncertainty (rather than the formal fitting error) in each coordinate is of order $0\overset{''}{.}2$. To check whether other emission was present in the H_2O channel maps, we used the aforementioned AIPS task SAD. We searched for any peaks with flux density above five times the 1σ rms noise level in each channel, which was between 36 and 54 mJy beam^{-1} for most channels except for ±4 channels around the channel with strongest emission (at 21.7 km s^{-1}) in which a value of 220 mJy beam^{-1} was found bearing witness to the excellent dynamic range in this (snapshot) observation. No emission was found except for that
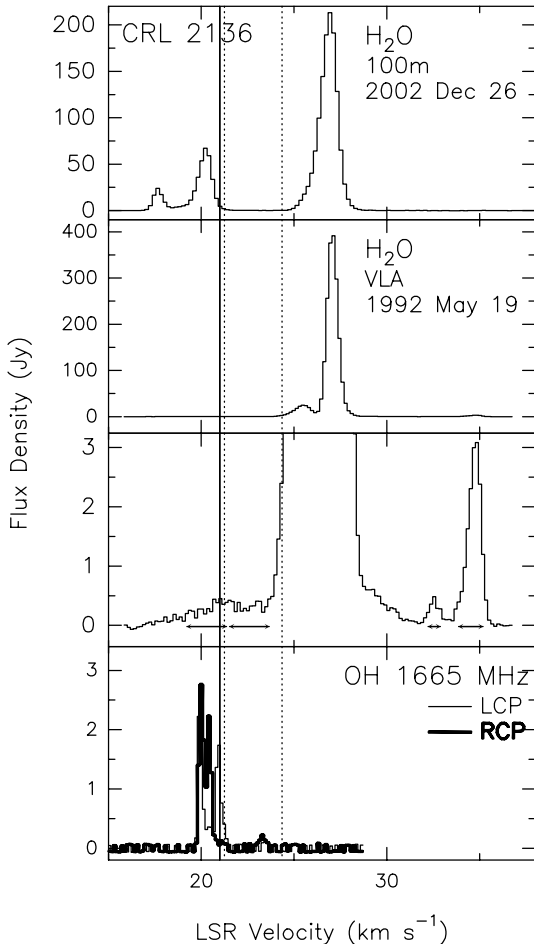
Fig. 3. *Top panel*: H$_2$O spectrum taken at the Effelsberg 100 m telescope on 2002 December 26. *Second panel from top*: VLA H$_2$O spectrum made from our 1992 May 19 data at the pixel with maximum emission. In the *third panel from top* the intensity axis is expanded to show the extremely weak emission at the lowest and highest velocities. The arrows show the velocity ranges over which maps of integrated emission, marked by the rectangles in Fig. 4 were produced. The *lower panel* shows the RCP and LCP emission of the OH 1665 MHz line published by Argon et al. (2000). For details of how the spectrum was formed see this reference. The dotted vertical lines mark the FWHM linewidths of various molecular species mapped by van der Tak et al. (2000b), who determine a centroid LSR velocity of 22.8(0.1) km s^{-1}. The solid line marks the velocity of the single, narrow 6.7 GHz CH$_3$OH maser feature (Caswell et al. 1995).

shown in Fig. 4, which covers an area of $\lesssim$10% of our FWHM synthesized beam width.

3. Discussion

3.1. OH and CH$_3$OH maser emission from the CRL 2136 hot core

The molecular hot core around CRL 2136 is characterized by elevated temperatures. For example, van der Tak et al. (2000a) find a methanol rotation temperature of 143 K, which is a lower limit to the kinetic temperature of the CH$_3$OH-emitting gas. However, the CH$_3$OH abundance is only 9×10^{-10} relative to H$_2$, 2 to 3 orders of magnitude below the solid-state abundances
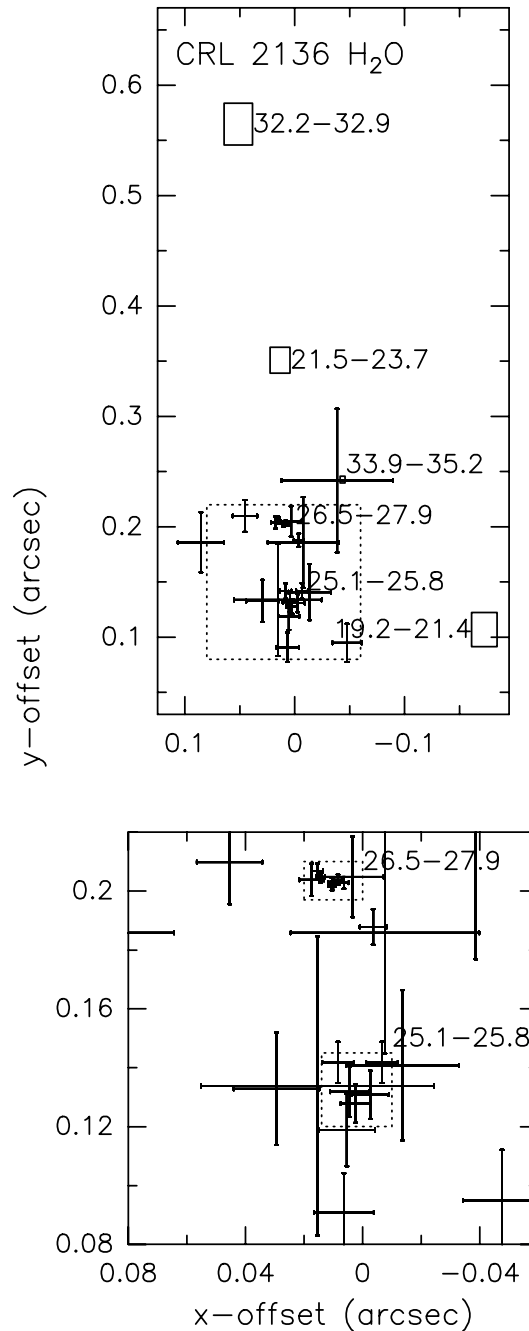

Fig. 4. Area containing the H$_2$O maser emission, indicated by the *dashed rectangle* in Fig. 1. The *error bars* in the *upper panel* give the positions of H$_2$O masers determined from channel by channel fitting of the H$_2$O data cube. The centers of the *full line* rectangles are the positions of the centroid positions of maps integrated over the velocity ranges given (and indicated in Fig. 3); the sizes corresponds to the 1σ errors of the fitted position. The *dotted rectangle* encloses the two regions of strongest emission, whose velocity ranges are given. This area is shown in more detail in the *lower panel*, in which the emission in the *dotted rectangles* spreads over the indicated velocities. Position offsets are relative to the position of RS 4 given in Table 1. Note that the relative registration of the H$_2$O and RS 4 have an estimated error of 0.3 arcsec.

and the gas-phase values found in other hot cores of similar temperature and difficult to explain, since CH$_3$OH evaporates

off grain mantles for temperatures exceeding ∼100 K (Sandford & Allamandola 1993). Possibly, a compact hot core with much higher CH_3OH abundance exists, but, if it has a diameter of, say, 1″ would have a much smaller filling factor in van der Tak et al.'s 14″ beam and would be "swamped" by more extended, lower methanol abundance material. Such a hot core would need to have much higher temperature than 143 K, because that value should in this case represent an "average" of the temperatures of the extended and hot core material.

Some insight may come from CH_3OH masers, which can be studied at milli-arcsecond resolution. As shown by Walsh et al. (2001) and Beuther et al. (2002b), class II CH_3OH masers are excellent tracers of deeply embedded massive and intermediate-mass stars, as well as of ultracompact HII regions. The 6.7 GHz class II CH_3OH maser emission toward CRL 2136 found by Macleod et al. (1992) in 1991 October/November consisted of a single, narrow ($\Delta v <$ 1 km s^{-1}), 25 Jy strong feature at the position listed in Table 1 and is, given its 10″ error in both coordinates coincident with our radio sources 3 and 4, although an identification with RS 4 seems more likely. Caswell et al. (1995) reobserved a virtually identical spectrum in 1992/1993. A more accurate position determination and high resolution mapping of the CRL 2136 CH_3OH maser, e.g. with Australia Telecope National Facility Compact Array [4], seem highly desirable.

Weak (1–2 Jy) OH maser emission was observed by Cohen et al. (1988) between ≈19 and 23 km s^{-1} in the 1665 and 1667 main hyperfine transitions and the former line was mapped using the VLA by Argon et al. (2000). The latter authors' positions are shown in the lower panel of Fig. 1. It is obvious that the OH, and by implication the class II CH_3OH masers probe the hot, dense environment in the immediate vicinity of RS 4. Other proof of this is the good agreement of the velocity spread of the lines from various species studied by van der Tak et al. (2000b).

The position of one 1665 GHz LCP feature (at 20.92 km s^{-1}) agrees to within 3 times the 1σ relative position uncertainly with that of an RCP feature at 20.42 km s^{-1}, indicating Zeeman-spitting. The derived B-field strength is 1 mG, which is a few times smaller than "typical" values one finds in interstellar OH maser regions.

To summarize the OH and CH_3OH maser data: The maser velocities suggest that they arise from the hot core surrounding IRS 1, but they are in a region further away (1000–4000 AU) from the heating source (IRS 1), in which temperatures (∼150 K) and densities (∼10^7 cm^{-3}) (see Menten 1997) are conducive for their excitation.

3.2. Radio source 4 and its environment

Although the relation of the intensity of the weak radio continuum emission detected in some high-mass protostars to their overall luminosity is at present not understood at all, it is clear that it represents a signpost for the exact position of the object and should, by means of theoretical modeling, give clues to its evolutionary state. Take the case of Orion-IRc2: here,

---

[4] http://www.atnf.csiro.au/

Table 2. Comparison: CRL 2136-RS4/Orion-KL (I).

	CRL 2136-RS 4	Orion-KL (I)
$S_{i,4.9}$ (mJy)	<0.48	–
$S_{i,8.4}$ (mJy)	0.56 ± 0.08	1.1 ± 0.2 [b]
$S_{i,14.9}$ (mJy)	1.3 ± 0.3	1.6 ± 0.4 [c]
$S_{i,43.2}$ (mJy)	4.2 ± 0.3	16 ± 2 [d]
$S_{i,86}$ (mJy)	61 ± 18 [e]	34 ± 5 [f]
θ_a (mas)	29^{+12}_{-29}	96 ± 10 [d]
θ_b (mas)	3^{+30}_{-3}	65 ± 9 [d]
major axis a (AU)	58	43
minor axis b (AU)	6	29
position angle (E of N)	116^{+32}_{-43}	146 ± 12 [d]

[a] $S_{p,\nu}$ and $S_{i,\nu}$ are the peak and integrated flux densities, respectively, determined with the AIPS task JMFIT. The upper limit is 3 times the 1σ rms noise. Source sizes were also determined using JMFIT and are discussed in the text.
[b] Menten & Reid (1995).
[c] Felli et al. (1993).
[d] Menten & Reid (in prep.).
[e] van der Tak et al. (2000b).
[f] Plambeck et al. (1995).

as shown by Menten & Reid (1995), the weak radio emission from source "I" almost certainly marks the position of the exciting object in the region, as the excitation of its surrounding SiO masers requires extreme temperatures and densities. Apart from the important signpost function, the detection of radio emission, which in the case of I is optically thick at least to a frequency of 43 GHz, can also put interesting constraints on the nature of the embedded protostar, as recently shown by Tan (2003), who proposes a jet model to explain I's radio emission. It should be noted that at the distance, D, of CRL 2136 (2 kpc), the detection of Orion source I (D = 450 pc) would require many hours of VLA time.

With regard to its low radio luminosity, rising spectrum, and likely connection with a powerful infrared source, RS 4 is similar to source I in Orion-KL (Table 2 and Fig. 5). The latter source's position in the centroid of SiO maser emission, which require high temperatures (∼1000 K) and densities (10^9 cm^{-3}) to be excited over the extent observed, makes it clear that it is the powering source in the region, providing the major portion of its luminosity of ∼10^5 $L_\odot$[5]. Also remarkable is that in Orion-KL the radio continuum/SiO emission is offset from the infrared source IRc 2, which represents reprocessed radiation, while the extinction toward the "real" source is so high to render it invisible even at the longest IR wavelengths accessible from the ground.

One may ask whether similar geometrical circumstances also apply to CRL 2136 and other infrared protostars. At first

---

[5] No SiO maser was found toward CRL 2136 by Kastner et al. (1992) in the 43.2 GHz v = 1, J = 1–0 transition to an rms noise level of 1 Jy. SiO maser emission has only been been detected in 3 star-forming regions, and in one of these, W51N (see Eisner et al. 2002) *only* in the v = 2, J = 1–0 transition.
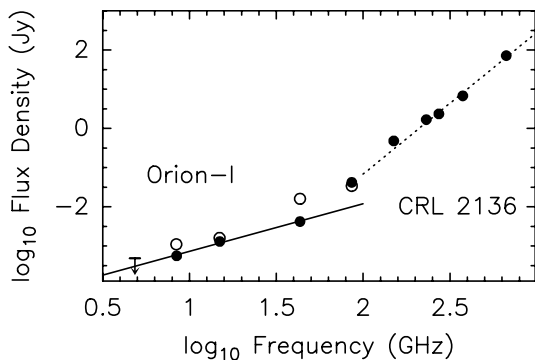
Fig. 5. The radio-to-submillimeter-wavelength spectral energy distributions of CRL 2136 IRS 1/RS 4 (*full dots*) and Orion source I (*open dots*). The *full line* represents a fit to our 4.9 to 43.3 GHz data for RS 4, while the *dashed line* is a fit to the submillimeter data of Kastner et al. (1994). Error bars of flux densities are smaller than or comparable to the symbol sizes.

sight, it certainly seems peculiar that some of the most massive compact dust emission sources are even detectable at near- and mid-IR wavelengths, and, moreover, shine as strong background sources for spectroscopy throughout that wavelength range, while others, such as the intermediate-mass protostar(s) W3(OH)-TW, are completely undetectable from the ground (Wyrowski et al. 1997, 1999; Stecklum et al. 2002). For the Willner et al. sources, the CO column densities in infrared absorption (pencil beam) and submm emission (15″ beam) differ by factors of 3 to 5, limiting the importance of geometry (van der Tak et al. 2000b).

What is the nature of the observed radio continuum emission from CRL 2136 (Fig. 5)? We derive a lower limit to the brightness temperature of 2020 K at 43.3 GHz, much higher than the dust sublimation temperature. RS 4's 8.4 to 14.9 GHz spectral index (SI), α_{XU} is 1.5; inclusion of the 43.3 GHz data point yields $\alpha_{XQ} = 1.2$ and we are, thus, in all likelihood seeing optically thick(ish) free-free emission up frequencies of 14.9 GHz, which becomes optically thinner at higher frequencies.

From the Kastner et al. (1994) 150 to 667 μm data we determine an SI, α_{submm} of 3.3, consistent with optically thin dust emission (Fig. 5). Extrapolation down to 86 GHz from the higher frequencies using this SI shows 95% of the 86 GHz flux density of 42 mJy can be accounted for by dust emission. Extrapolation of the cm-data (using $\alpha_{XQ} = 1.2$) yields 17 mJy, indicating a flattening of the radio spectrum. As Table 2 and Fig. 5 demonstrate, RS 4 and I share a number of characteristics: both have elongated, jet-like morphology, rising radio spectra that flatten above 30 GHz, and even comparable physical dimensions.

Motivated by Orion source I's elongated morphology, Tan (2003) models this source as a double jet, powered by accretion onto a protostar. For accretion rates above 10^{-4} $M_\odot$ yr^{-1} he finds the flux densities at $\nu \lesssim 30$ GHz to be insensitive to the accretion rate and to grow as ν^2, while the spectrum flattens at higher frequencies and a ν^2 dependence up to 86 GHz seems to require $\dot{M}_{in} > 5 \times 10^{-4}$ $M_\odot$ yr^{-1}, a very high value. Maybe this

model can be taken as a starting point for further studies trying to explain the radio emission from IRS 1/RS 4. Differences between RS 4 and I are the former source's ∼10 times higher lower frequency radio luminosity and the lower turnover frequency. Reynolds (1986), modeling collimated ionized stellar winds, finds that an SI of 1.2 requires recombination or acceleration in the flow.

Neufeld & Hollenbach (1996) have calculated the free-free emission emerging from an accretion shock for different protostellar masses, M, and infall rates $\dot{M}_{in}$. Alas, even for the most extreme cases they considered, $M = 10$ $M_\odot$ (solar masses) and $\dot{M}_{in} = 10^{-4}$ $M_\odot$ yr^{-1}, the 4.8 and 8.4 GHz flux densities they obtained, scaled to $D = 2$ kpc, are more than a factor of hundred lower than the flux densities we measure at these frequencies, making this mechanism extremely unlikely.

3.3. CRL 2136's compact water maser emission

The three most salient observational facts of the H$_2$O maser emission from RS 4 are: first, the strongest H$_2$O maser mission is redshifted relative to the systemic velocity of 22.8 km s^{-1}. Second, the centroid position of the H$_2$O emission has a formal offset of $(\theta_x, \theta_y) = (+0.01, +0.15)$ from, and thus is within the errors *coincident* with RS 4, and third, *all* of the H$_2$O emission is within the small rectangle of size 0.″3 × 0.″5 (600 × 1000 AU) outlined in Fig. 1 and shown in detail in Fig. 4. It seems worth mentioning that the strongest ($S > 10$ Jy) emission arises from two compact regions, separated in NS direction by 0.″07 (=140 AU).

Assuming, first, that the LSR velocity of the protostar is identical to that of its surrounding hot core, and, second, that either of the compact strong emission regions is spatially coincident with the continuum source, the observed redshift of the strong H$_2$O emission means that we are observing infall of the water-containing material onto the protostar. The fact that the continuum emission is optically thick naturally explains the predominance of red-shifted H$_2$O emission.

If the above were true, the case of CRL 2136 would be a convincing case of water maser emission emerging from *inflowing* circum-(proto)stellar gas. There is abundant evidence for interstellar maser emission associated with bipolar molecular *outflows*, both, from the frequently observed extreme velocity ranges (often ± tens of km s^{-1} around the systemic velocity or more) and from direct proper motion determinations (see, e.g., Reid & Moran 1988). For the (outflow) cases, excitation calculations place the water in the postshock regions of J-shocks, where densities are a few times 10^8–10^9 cm^{-3}, the temperature is ∼400 K, and the water abundance is enhanced in the postshock chemistry (Elitzur et al. 1989).

Given the fact that H$_2$O masers are "usually" outflow tracers *par excellence* we speculate, hesitantly, but excitedly, that the redshifted H$_2$O maser emission moving onto CRL 2136 is produced in the postshock gas behind the accretion shock. Neufeld & Hollenbach (1996) consider accretion shock velocities of 30 km s^{-1} or higher, much smaller than the values indicated by our emission.

Given that CRL 2136 drives a massive outflow (with 50 $M_\odot$ in the outflowing gas), mapped in the CO molecule by Kastner et al. (1994), it is curious that we do not see any water emission at all that is associated with the outflow, given the ubiquity of H$_2$O maser emission observed from outflows from stars of all masses[6]. Most regions, placed at CRL 2136's distance, would show copious H$_2$O emission within several to (in Orion-KL) several tens of arcseconds from the exciting source. This H$_2$O maser/accretion shock scenario is certainly speculative and has one obvious weakness: given the dimensions of the continuum emission region only one, but not both of the regions with strong redshifted H$_2$O emission regions can be coincident with the continuum. This assumes that the continuum source has the same size at 22.2 GHz, where the emission is optically thick, as at 43.3 GHz, where it is becoming optically thin. Moreover, there is the detection of blueshifted emission in the Effelsberg spectrum 1000 AU from the star, which is clearly inconsistent with a pure accretion shock scenario, necessitating the assumption of an additional outflow component. Actually, not only the blueshifted H$_2$O masers must be outflowing, but also some of the redshifted ones, else a very high central mass is required.

Finally, we would like to mention that Fiebig (1997) modeled the water emission emission observed toward the FU Orionis star L1287 as clumps falling on the accretion disk, trying to explain the observed velocity distribution. We have not explored whether our H$_2$O observations could be explained by a variation of his model.

3.4. Interstellar water masers not associated with bipolar outflows

It is clear from the observed wide radial velocity ranges, elongated emission distributions, and, most persuasively, measured proper motions that at least many, if not the majority of interstellar H$_2$O masers are formed in, mostly bipolar, outflows (Reid & Moran 1988). Particularly collimated examples include W49 and W3(OH)-H$_2$O (Gwinn et al. 1992; Alcolea et al. 1993). A model for masers with this morphology was presented by Mac Low & Elitzur (1992) and Mac Low et al. (1994).

In many cases where masers in both OH and H$_2$O were mapped, the masers in the two species are frequently found in the same regions on a, say, 0.1 pc scale. However, on smaller scales one mostly finds distinctly different distributions for the two species. Moreover, in most cases OH maser emission covers a significantly smaller velocity range as H$_2$O emission, indicating that it emerges from the slowly (a few km s^{-1}) outmoving or infalling envelopes of young stars; in some cases,

e.g. W3(OH), from just outside the ionization/shock front of an UCHII region (Reid et al. 1980)[7].

Given the completely different pumping requirements of H$_2$O and OH masers ($n \sim 10^9$ cm^{-3}/$T \sim 400$ K; Elitzur et al. 1989) and ($\sim 10^7$ cm^{-3}/~ 150 K; Cesaroni & Walmsley 1991), respectively, it is clear that both masers arise in quite different gas volumes (n and T are density and kinetic temperature, respectively). The apparently contradictory result that H$_2$O masers occur further away from their exciting sources than OH masers is explained by the fact that they arise from hot, compressed postshock material. Also, cases were OH and H$_2$O masers appear on the same spot in the sky may be chance projections.

That the CRL 2136 maser is located so close (closer than the OH masers) to the exciting source, as well as its velocity structure, indicates that we are dealing with a maser that is *not* associated with an outflow, but, as discussed above, possibly with infall. This interpretation is corroborated by the absence of high-velocity H$_2$O emission. Could a whole class of such H$_2$O masers exist, which are clearly identified on observational grounds, but whose "distinction" from outflow-associated masers has not yet been recognized? We consider this to be entirely conceivable. Inspection of the OH and H$_2$O maps of Forster & Caswell (1999) reveals a number of candidate sources that sometimes, although not always, are associated with weak contiunuum emission.

Another source showing a very similar relationship between H$_2$O masers and a weak, compact, and elongated radio continuum source as CRL 2136 is AFGL 2591 (Trinidad et al. 2003), an infrared source of comparable luminosity to CRL 2136 [2 × 10^4 $L_\odot$ (assuming $D = 1$ kpc) compared to CRL 2136's 5 × 10^4 $L_\odot$]. Here the H$_2$O masers are concentrated in a $\sim$60 AU region.

We also mention the remarkable H$_2$O maser distribution mapped by Torrelles et al. (2001) toward Cepheus AHW2, which to great accuracy traces part of a circular arc (of radius 62 AU), indicating spherical, episodic ejection. Recently, this arc was found to be expanding (Gallimore et al. 2003). Other regions with extremely compact H$_2$O maser distributions (more compact than CRL 2136's 600 × 1000 AU) are NGC 2071-IRS3 (40 AU possibly in a disk; Torrelles et al. 1998), and W75 N(B) (150 AU; Torrelles et al. 1997).

Finally, we mention that in Orion-KL, Genzel et al. (1980) identify, in addition to a high- and a low-velocity H$_2$O outflow, the so-called "shell" masers[8], which only occur in the immediate vicinity of IRc 2 (=source I) and have apparent maser spot

---

[6] The poorly collimated CO outflow is along a position angle of $\sim$135° over a $\sim$80″ × 80″ (0.8 × 0.8 pc) area, with the blueshifted gas SE and the redshifted NE of IRS 1. There is little correspondence with our H$_2$O maser distribution (Fig. 4), other than that we also observe redshifted emission N of the blueshifted emission, although at 200 times smaller scale.

[7] While this picture for interstellar OH masers probably holds for the majority of the stronger sources, recently weak OH maser emission has also been identified offset from the UCHII/OH maser source W3(OH), whose position places it at the working surface of the H$_2$O maser outflow that originates from a deeply embedded protostar neighboring the former region (Argon et al. 2003).

[8] These masers are called "shell-type" by Genzel et al. because their velocity structure resembles that of H$_2$O masers in evolved star circumstellar shells. These masers are "resolved out" by Genzel et al.'s and other high-resolution VLBI observations, although the latter authors give Hansen (1980) as a VLBI reference. A good VLA A-array map of the Orion H$_2$O masers seems highly desirable!

sizes that are an order of magnitude larger than any other maser in the Orion region. These masers may be the archetype of the new class identified here.

4. Conclusions and outlook

Using the VLA, we have detected several weak radio continuum sources in the CRL 2136 region. One of these, RS 4, is, within the errors, coincident with IRS 1, the high-mass protostar exciting the region. Taking our 8.4, 14.9, and 43.3 GHz data and 86 GHz data from the literature, the emission, which is almost certainly free-free radiation, has a rising spectral index, α ($S \propto \nu^\alpha$) of 1.2 up to 43.3 GHz, which flattens at higher frequencies. The continuum emission might be arising from a bipolar jet, as modeled by Tan (2003), and it seems highly desirable to apply his model to the region discussed here.

Water maser emission was found from a very confined region of size $0\rlap{.}''3 \times 0\rlap{.}''5$ (600×1000 AU) with its centroid coincident with RS 4. All of the strong emission is redshifted relative to the systemic velocity by up to 4 km s^{-1}. The strongest emission arises from a single feature (at $v_{peak} = 27.1$ km s^{-1}), which appears to have been at the same velocity (to within $\approx \pm 0.1$ km s^{-1}) for a period of at least 9 years. Given the observed redshift, it is interesting to speculate that the water-containing gas giving rise to the strong emission is falling onto the central protostar and is boosted by amplification of the background continuum emission. Given the measured size of the continuum emission region ($0\rlap{.}''029 \times 0\rlap{.}''003$) this can only be true for part of the strong emission, which is arising from two compact regions $0\rlap{.}''08$ apart. *Simultaneous* high ($<0\rlap{.}''1$) resolution VLA observations of the H₂O maser emission and the 22 GHz continuum emission will provide a detailed picture of the relationship between the two phenomena (reducing the cross-registration uncertainty to a few milli-arcseconds) and certainly prove or disprove the accretion shock scenario. Using the H₂O maser as a phase reference (Reid & Menten 1990, 1997) will allow very high quality imaging.

The accretion shock seems a natural environment for the production of the H₂O maser emission, which requires temperatures around 400 K and densities between 10^8 and 10^9 cm^{-3}. Modeling efforts should explain the velocity stability of the strong maser feature. The model of free-free emission from accretion shocks by Neufeld & Hollenbach (1996) under-predicts the observed radio continuum by several orders of magnitude.

Finally, we speculate that the CRL 2136 H₂O masers belong to a not yet identified class of H₂O masers that are in the closest vicinity of the protostar and do not partake in outflows, but possibly are part of the infalling material. The prototype of this class are the "shell-type" masers in Orion-KL.

References

Alcolea, J., Menten, K. M., Moran, J. M., & Reid, M. J. 1993, in Astrophysical masers, ed. A. Clegg, & G. Nedoluha (Berlin: Springer), 225

Argon, A. L., Reid, M. J., & Menten, K. M. 2000, ApJS, 129, 159

Argon, A. L., Reid, M. J., & Menten, K. M. 2003, ApJ, 593, 925

Baars, J. W. M., Genzel, R., Pauliny-Toth, I. I. K., & Witzel, A. 1977, A&A, 61, 99

Beuther, H., Schilke, P., Menten, K. M., et al. 2002a, ApJ, 566, 945

Beuther, H., Walsh, A., Schilke, P., et al. 2002b, A&A, 390, 289

Caswell, J. L., Vaile, R. A., Ellingsen, S. P., Whiteoak, J. P., & Norris, R. P. 1995, MNRAS, 272, 96

Cesaroni, R., & Walmsley, C. M. 1991, A&A, 241, 537

Churchwell, E. 2002, in Hot Star Workshop III: the Earliest Stages of Massive Star Birth, ed. P. A. Crowther (San Francisco: ASP), ASP Conf. Proc., 267, 3

Cohen, R. J., Baart, E. E., & Jonas, J. L. 1988, MNRAS, 231, 205

Eisner, J. A., Greenhill, L. J., Herrnstein, J. R., Moran, J. M., & Menten, K. M. 2002, ApJ, 569, 334

Elitzur, M., Hollenbach, D. J., & McKee, C. F. 1989, ApJ, 346, 983

Felli, M., Taylor, G. B., Catarzi, M., Churchwell, E., & Kurtz, S. 1993, A&AS, 101, 127

Fiebig, D. 1997, A&A, 327, 758

Forster, J. R., & Caswell, J. L. 1999, A&A, 137, 43

Gallimore, J. F., Cool, R. J., Thornley, M. D., & McMullin, J. 2003, ApJ, 586, 306

Garay, G., & Lizano, S. 1989, PASP, 111, 1049

Genzel, R., Reid, M. J., Moran, J. M., & Downes, D. 1980, ApJ, 224, 884

Gwinn, C. R., Moran, J. M., & Reid, M. J. 1992, ApJ, 393, 149

Hansen, S. S. 1980, Ph.D. thesis, Univ. of Mass., Amherst

Kastner, J. H., & Weintraub, D. A. 1996, ApJ, 466, L103

Kastner, J. H., Weintraub, D. A., & Aspin, C. 1992, ApJ, 389, 357

Kastner, J. H., Weintraub, D. A., Snell, R. L., et al. 1994, ApJ, 425, 695

MacLeod, G. C., & Gaylard, M. J. 1992, MNRAS, 2567, 519

Mac Low, M., Elitzur, M., Stone, J. M., & Konigl, A. 1994, ApJ, 427, 914

Mac Low, M., & Elitzur, M. 1992, ApJ, 393, L33

Menten, K. M. 1997 in Molecules in Astrophysics – Probes, & Processes, ed. E. van Dishoeck (Dordrecht: Kluwer), IAU Symp., 178, 163

Menten, K. M., & Reid, M. J. 1995, ApJ, 445, L157

Mitchell, G. F., Maillard, J.-P., Allen, M., Beer, R., & Belcourt, K. 1990, ApJ, 371, 342

Mitchell, G. F., Maillard, J.-P., & Hasegawa, T. I. 1991, ApJ, 371, 342

Molinari, S., Brand, J., Cesaroni, R., & Palla, F. 1996, A&A, 308, 573

Molinari, S., Brand, J., Cesaroni, R., & Palla, F. 2000, A&A, 355, 617

Molinari, S., Brand, J., Cesaroni, R., Palla, F., & Palumbo, G. G. C. 1998, A&A, 336, 339

Moran, J. M. 1998, Proc. SPIE, 3357, 208

Neufeld, D. A., & Hollenbach, D. J. 1996, ApJ, 471, L45

Plambeck, R. L., Wright, M. C. H., Mundy, L. G., & Looney, L. W. 1995, ApJ, 455, L189

Reid, M. J., Argon, A. L., Masson, C. R., Menten, K. M., & Moran, J. M. 1995, ApJ, 443, 238

Reid, M. J., Haschick, A. D., Burke, B. F., et al. 1980, ApJ, 1980, 239

Reid, M. J., & Moran, J. M. 1988, in Galactic and extragalactic radio astronomy, 2nd edition (Berlin and New York: Springer), 255

Reid, M. J., & Menten, K. M. 1990, ApJ, 360, L51

Reid, M. J., & Menten, K. M. 1997, ApJ, 476, 327

Reynolds, S. P. 1986, ApJ, 304, 713

Sandford, S. A., & Allamandola, L. J. 1993, ApJ, 417, 815

Sridharan, T. K., Beuther, H., Schilke, P., Menten, K. M., & Wyrowski, F. 2002, ApJ, 566, 931

Stecklum, B., Brandl, B., Henning, Th., Pascucci, I., Hayward, T. L., & Wilson, J. C 2002, ApJ, 392, 1025

Tan, J. C. 2003 in Galactic Star Formation across the Stellar Mass Spectrum, ed. J. M. de Buizer, & N. S. van der Bliek (San Francisco: ASP), 207

Torrelles, J. M., Gomez, J. F., Rodriguez, L. F., et al. 1997, ApJ, 489, 744

Torrelles, J. M., Gómez, J. F., Rodríguez, L. F., et al. 1998, ApJ, 505, 756

Torrelles, J. M., Patel, N. A., Gómez, J. F., et al. 2001, Nature, 411, 277

Tieftrunk, A. R., Gaume, R. A., Claussen, M. J., Wilson, T. L., & Johnston, K. J. 1997, A&A, 318, 931,

Trinidad, M. A., Curiel, S., Cantó, J., et al. 2003, ApJ, 589, 386

Valdettaro, R., Palla, F., Brand, J., et al. 2001, A&A, 368, 845

van der Tak, F. F. S., van Dishoeck, E. F., Caselli, P. 2000a, A&A, 361, 327

van der Tak, F. F. S., van Dishoeck, E. F., Evans, N. J., II, & Blake, G. A. 2000b, ApJ, 537, 283

van der Tak, F. F. S., Boonman, A. M. S., Braakman, R., & van Dishoeck, E. F. 2003, A&A, 412, 133

van Dishoeck, E. F., Aelmich, F. P., Schutte, W. A., et al. 1998, in Star Formation with the Infrared Space Observatory, ed. J. L. Yun, & R. Liseau (San Francisco: ASP), ASP Conf. Ser., 132, 54

Walsh, A., Bertoldi, F., Burton, M. G., & Nikola, T. 2001, MNRAS, 326, 36

Wilner, D. J., Reid, M. J., & Menten, K. M. 1999, ApJ, 513, 775

Willner, S. P., Gillett, F. C., Herter, T. L, et al. 1982, ApJ, 253, 174

Wood, D. O. S., & Churchwell, E. 1989, ApJS, 69, 831

Wyrowski, F., Hofner, P., Schilke, P., et al. 1997, A&A, 320, L17

Wyrowski, F., Schilke, P., Walmsley, C. M., & Menten, Karl M. 1999, ApJ, 514, L43